Multilevel Peel-off Patterning of a Prototype Semitransparent Organic Photovoltaic Module

Xinjing Huang[1], Dejiu Fan[2], Yongxi Li[2] and Stephen R. Forrest[1,2,3,*]

1.Applied Physics Program,

2. Department of Electrical Engineering and Computer Science,

3. Department of Physics, Department of Material Science and Engineering

University of Michigan, Ann Arbor, MI, 48109 United States

**Corresponding author and lead contact: stevefor@umich.edu*

Summary

Semitransparent organic photovoltaics (ST-OPVs) with applications to power generating windows have shown substantial increases in power conversion efficiency (*PCE*) and average photopic transmission (*APT*) at the laboratory scale. The demonstration of similarly efficient, large-scale ST-OPV modules with geometric fill factors (*GFF*) approaching 100%, however, remains a challenge. Here, we employ a multilevel peel-off patterning method that can achieve micron-scale resolution without exposing chemically sensitive organic materials to solvents. Eight, 4 cm × 0.4 cm cells are connected in series to realize a prototype ST-OPV module with *GFF* = 95.8%, with *PCE* = 7.3 ± 0.2% under simulated AM 1.5G illumination at 1 sun intensity, *APT* = 41.8 ± 1.4%, and a light utilization efficiency of *LUE* = 3.1 ± 0.1%. A neutral color ST-OPV module is also demonstrated with 1.7 ± 0.1% and International Commission on Illumination (CIE) LAB coordinates of (L*, a*, b*) = (53.7, -1.9, -3.9).

Introduction

Organic semiconductors are being employed for a range of modern photonic and electronic devices due to their distinct advantages of low cost, light weight, flexibility, and environmental compatibility.[1] The past few decades have witnessed remarkable developments in the performance of such devices as organic light emitting diodes (OLEDs), organic photovoltaics (OPVs) and organic thin film transistors (OTFTs). An essential step to realize high volume production of electronic devices is high-resolution patterning techniques.[2–6] While small, laboratory-scale OPVs have demonstrated high power conversion efficiency (*PCE*) with exceptional stability, OPV modules can also benefit from high-resolution patterning, although this has attracted considerably less attention.[7–12] In particular, OPVs show considerable promise for use in power generating windows due to their transparency across the visible spectrum along with selective absorption in the near-infrared (NIR); a feature resulting from the relatively narrow excitonic absorption spectra of organic semiconductors.[13–15] To date, semitransparent OPVs (ST-OPVs) exhibit a light utilization efficiency of $LUE = PCE \times APT$ as high as 5%. Here, *APT* is the average photopic transmission.[16–23] To realize practical applications, scalable fabrication processes of modules with minimal loss in power generation need to be established. Considerable loss in OPV module efficiencies, and visible artifacts in ST-OPVs arise from the large area consumed by interconnections between constituent cells. Such deficiencies can be significantly reduced by high-resolution patterning.

Conventional module patterning based on mechanical scribing, shadow masking, gravure printing, slot-die coating, etc.[24–31] often yield interconnection widths at the millimeter scale, and result in a low geometric fill factor, *GFF*, which is the ratio between the active cell and the total module areas. In contrast, laser ablation has achieved interconnection widths of hundreds of microns.[32–38] However, ablation can result in damage to the surrounding and materials comprising the device.[35,39] Moreover, the illumination wavelength and pulse durations must be tailored to ablate only the targeted materials.[33,35] As a result of these limitations, the highest efficiency opaque OPV modules fabricated with laser ablation have shown approximately 10% *PCE* loss compared to laboratory-scale devices.[35,38,40]

An alternative to these methods is photolithographic patterning. However, commonly used photoresists contain solvents that can degrade chemically sensitive organic materials. Moreover, lithographic patterning and photoresist removal can also employ reactive ion or solvent-based wet chemical processes that can damage organic semiconductors. In this work, we employ a patterning method that combines a non-destructive polymer-based peel-off patterning of ST-OPV modules with photolithographic resolution.[41–47] The general elements of the peel-off patterning process are provided in Fig. 1(a). A polymer is first coated on the substrate and patterned into long, narrow strips with conventional photolithography. The choice of the polymer includes, but is not limited to polyimide (PI), parylene, etc. After photoresist removal, the organic layer to be patterned is deposited and the polymer strips are mechanically peeled off, removing the organic on their surfaces from the

module. Figure 1(b) shows a microscopic image of the organic blend film on a glass substrate patterned by peeling off a 10 μm wide PI strip. The wedge at the edge of the PI strip is picked up to initiate the peel-off. In the method of Fig. 1, multilevel peel-off produces large scale features with micron-scale resolution. Moreover, this method is independent of the details of the organic materials system or layering scheme, and does not damage the chemically sensitive active layers.

Similar methods have been employed in the patterning of biological materials,[41–44] organics,[45,46] and perovskites.[47] Most of these demonstrations focus primarily on the patterning of micron-scale features with a single level patterning step utilizing one polymer layer to pattern one target layer. To achieve complicated device structures and circuit interconnection in a module, however, multi-step/multilevel peel-off patterning over large substrate areas is essential. In recent work that employs multi-step peel-off patterning, multiple polymer layers are repeatedly deposited and lithographically removed over chemically sensitive materials, which severely degrades the device performance.[45,47]

Here, we demonstrate multilevel peel-off patterning scheme in the fabrication of prototype opaque and semitransparent OPV mini-modules with *GFF* = 95.8% comprising eight, series connected 4 cm × 0.4 cm cells separated by 200 μm wide interconnections. A schematic illustration of the completed module is shown in Fig. 1(c). The opaque OPV module reaches *PCE* = 10.3 ± 0.3% under simulated AM 1.5G illumination at 1 sun intensity, which is only 5% less than an analogous 4 mm^2 device. Combined with an ultrathin Ag top electrode and a visible light out-coupling (OC)

structure, the ST-OPV module exhibits *LUE* = 3.1 ± 0.1% with *PCE* = 7.3 ± 0.2% and *APT* = 41.8 ± 1.4%. The module has a blue-green tint with International Commission on Illumination (CIE) LAB coordinates of (L*, a*, b*) = (70.9, -11.3, -7.5). In addition, a color-neutral ST-OPV module is demonstrated with *LUE* = 1.7 ± 0.1% and (L*, a*, b*) = (53.7, -1.9, -3.9).

Results and Discussion

Figure 2 details the step-by-step patterning procedure to realize series connection between individual OPV cells. The indium tin oxide (ITO) bottom cathode is photolithographically patterned into 4.15 mm wide strips, and a PI layer is coated onto the electrodes. The PI is patterned into parallel, 50 μm and 75 μm wide strips via photolithography. As shown in Fig. 2(a), there are pairs of 50 μm and 75 μm PI strips with 50 μm separation at the edge of each cathode strip. Next, the ZnO and MoO_x charge transport layers as well as the ternary bulk heterojunction (BHJ), comprising a blend of the narrow energy gap polymer donor, PCE-10, and two NIR-absorbing acceptors, BT-CIC and TT-FIC (see Supplemental Information for IUPAC nomenclatures of the molecules employed), are deposited, see Fig. 2(b).[16] The 75 μm wide strips between two adjacent bottom cathodes are peeled off to separate the charge transport layers and the BHJs of adjacent devices. This exposes a portion of the bottom electrodes to allow series connection between cells, as shown in Fig. 2(c). Finally, the Ag anode is deposited, and the remaining 50 μm wide polymer strips are subsequently peeled off to separate the top electrodes of two adjacent devices, see Figs. 2(d) and (e). The microscopic image in Fig. 2(e) shows the 200 μm wide interconnection between

two individual OPV cells (see Fig. S1 for the profilometry profile), featuring clean pattern edges.

In the module, a narrow individual cell width reduces the *GFF*, while a large width results in increased series resistance loss from the transparent electrodes. Here, the width of individual device is limited to 4 mm to minimize the total loss from both the *GFF* and series resistance,[35,48,49] and the length of each cell is 4 cm. The modules have 12.8 cm^2 active area for a total module area of 13.34 cm^2, and *GFF* = 95.8%. Note that, for 10 μm wide PI strips as demonstrated in Fig. 1(b), the interconnection distance could potentially be reduced to 40 μm, giving *GFF* = 99.1%. Furthermore, the resolution and dimension of this patterning method depends on the tensile strength of the polymer and the stress applied to the strip during peeling, since as it will break if the latter exceeds the former. Therefore, the possibility of failure during peeling is higher when the strip is narrower and longer. These limitations can potentially be circumvented in meter-scale modules patterned at resolutions of tens of microns, for example, by employing a roller to continuously release the stress along the polymer strip during removal (Figure S2).

To study the feasibility of the patterning method, we fabricated an opaque OPV module and an analogous 4 mm^2 device comprising a 150 nm thick indium tin oxide (ITO) bottom cathode, an 80 nm thick PCE-10:BT-CIC:TT-FIC (1:1.25:0.5, w/w/w) blended ternary BHJ, 30 nm thick ZnO and 20 nm thick MoO_x as electron and hole transporting layers, respectively, and a 150 nm thick Ag anode (see supplemental experimental procedures). The performance parameters are listed in Table 1 (see Figure

S3 for device structure and performance data). The module achieves short circuit current I_{SC} = 36.7 ± 0.6 mA, open circuit voltage V_{OC} = 5.42 ± 0.02 V, fill factor *FF* = 0.66 ± 0.01, and *PCE* = 10.3 ± 0.3%. Compared to the 4 mm^2 device, the module shows negligible loss in I_{SC} (individual cell area 1.6 cm^2, with an average short circuit current density of J_{SC_AVG} = 22.9 mA/cm^2) and V_{OC}, while the *FF* decreases from 0.69 ± 0.01 to 0.66 ± 0.01, which is primarily due to resistance losses from the ITO cathode. Since peel-off does not introduce damage to the materials comprising the devices, the module *PCE* shows only a 5% decrease compared to the 4 mm^2 device.

The ST-OPVs were fabricated by substituting the thick Ag anode with an ultrathin 16 nm Ag layer, and integrating a 4-layer outcoupling structure comprising CBP (50 nm)/MgF_2 (100 nm)/CBP (80 nm)/MgF_2 (10 nm) (see supplemental experimental procedures),[16,21] as illustrated in Fig. 3(a). Figure 3(b) shows the current density-voltage (*J-V*) and current-voltage (*I-V*) characteristics of the 4 mm^2 ST-OPV devices and modules with and without the OC structure. The external quantum efficiency (*EQE*), transmission, and reflection spectra of the devices are plotted in Figs. 3(c) and (d), with detailed performance parameters provided in Table 1. The ST-OPV modules show negligible loss in I_{SC} and V_{OC} compared to the analogous 4 mm^2 devices. The ultrathin Ag top anode introduces additional resistance loss due to its limited conductivity. This results in a reduction in *FF* from 0.70 ± 0.01 to 0.64 ± 0.01. Figure 3(d) shows that the transmission of ST-OPV device without an OC structure has a peak at a wavelength of λ = 430 nm, followed by a significant decrease at λ > 500 nm due to the absorption by the device. To improve the *APT*, an OC structure was employed to maximize the

transmission of visible wavelengths via control of interference peaks in the multilayer stacks.[16] It enhances the transmission between 400 nm and 600 nm, with a peak at 560 nm, which is close to the peak photopic response of the eye. Therefore, the OC structure significantly improves the *APT* from 22.3 ± 1.1% to 41.8 ± 1.4%. However, the increase in transparency leads to a reduction of I_{SC} from 28.2 ± 0.7 mA to 27.2 ± 0.5 mA, as shown by the decreased *EQE* in Fig. 3(c). As a result, the ST-OPV module with the OC structure exhibits *PCE* = 7.3 ± 0.2% with high reproducibility (Figure S4) and reaches *LUE* = 3.1 ± 0.1%.

A photographic image of the module with OC structure is shown in Fig. 3(e). The module area (outline with a black dashed box) shows a transparent, tint and narrow, bright lines from transmission through the gaps in the interconnection regions. This effect can be reduced, either by increasing the *APT* to reduce the contrast between the active and interconnection areas, or by patterning narrower stripes. Ideally, modules used as window panels should transmit light as close to neutral color as possible, which requires (a*, b*) coordinates in the CIELAB color space that approach (0, 0). The ST-OPV module with OC exhibits CIELAB coordinates (L*, a*, b*) = (70.9, -11.3, -7.5), which accounts for its blue-green tint.

To realize neutral color ST-OPV modules, we employed a 4-layer optical structure consisting of CBP (45 nm)/ZnS (45 nm)/CBP (110 nm)/MgF_2 (10nm), as illustrated in Fig. 4(a), whose *J-V* and *I-V* characteristics are shown in Fig. 4(b), with detailed performance parameters listed in Table 1. The module exhibits I_{SC} = 27.6 ± 0.4 mA, V_{OC} = 5.34 ± 0.02 V and *FF* = 0.64 ± 0.01, which yields *PCE* = 7.4 ± 0.2%. The *EQE*,

transmission and reflection spectra are plotted in Fig. 4(c). Compared to the device without the OC structure, the transmission of neutral color ST-OPV decreases between λ = 400 nm and 500 nm, and increases between 550 nm and 650 nm, to reach a balance over the visible region. The neutral color module achieves (L*, a*, b*) = (53.7, -1.9, -3.9), a high color rendering index of 88, and a correlated color temperature of 5944 K, which is close to the solar surface temperature of 5776K. The *APT* and *LUE* of the module are 22.8 ± 1.3% and 1.7 ± 0.1%, respectively. Figure 4(d) shows a photographic image with the module area bordered by a black dashed box. The illumination through the module can accurately render the colors of white, red, green and blue in the background.

Note that the mini-modules fabricated using peel-off are, to our knowledge, the first demonstration of OPV modules that overcomes the considerable *PCE* loss observed in other high resolution patterning processes. Its resolution suggests that the strips can be made even narrower than demonstrated, leading to *GFF* approaching unity.

Finally, while we cannot make a precise comparison between the costs of peel-off patterning and the widely used laser ablation patterning, a large capital expenditure in laser patterning arises from the acquisition of precise, large-scale laser ablation tools, whose illumination wavelength may have to be adjusted for specific materials and device structures. In contrast, the photolithographic tools used in peel-off patterning are standard in semiconductor and OLED processing lines, thus reducing the cost of capital and depreciation. However, the peel-off method requires additional costs of materials used for the polymer patterning layer and in the photolithographic processes, which

scale with the size of the solar panels. An accurate comparison of costs admittedly warrants further study which is beyond the scope of this demonstration.[50]

Conclusion

In this work, we introduced a peel-off patterning technique that can achieve micron-scale patterning resolution of organic materials without introducing damage incurred using conventional photolithography. Using this method, we fabricated prototype, series-connected OPV modules with 12.8 cm^2 active area and $GFF = 95.8\%$. An opaque OPV module was demonstrated with $PCE = 10.3 \pm 0.3\%$, which features a remarkably small *PCE* loss of only 5% compared to analogous 4 mm^2 devices. ST-OPV modules were fabricated by utilizing ultrathin Ag top electrode and an OC structure. The optimized ST-OPV module achieves $LUE = 3.1 \pm 0.1\%$ with $PCE = 7.3 \pm 0.2\%$ and $APT = 41.8 \pm 1.4\%$. Furthermore, we demonstrated a neutral color ST-OPV module with $LUE = 1.7 \pm 0.1\%$ and (L*, a*, b*) = (53.7, -1.9, -3.9). The peel-off patterning technique introduces the possibility for realizing ST-OPV modules with high efficiency and *GFF* approaching 100% over large areas. Our result is general in that it shows a potential path for multilevel, high-resolution patterning with micron-scale resolution of chemically sensitive organic electronic materials over large areas.

Resource Availability

Lead Contact

Further information and requests for resources and materials should be directed to and will be fulfilled by the lead contact, Stephen R. Forrest (stevefor@umich.edu).

Materials Availability

This study did not generate new unique materials.

Data and Code Availability

The data that support this study are available from the lead contact upon reasonable request.

Supplemental Information

Document S1. Figure S1-S4, supplementary experimental procedures.

Data S1. Standardized data reporting for photovoltaic cells.

Acknowledgements

This work is supported by the U.S. Department of Energy's Office of Energy Efficiency and Renewable Energy (EERE) under Solar Energy Technologies Office (SETO) Agreement Number DE-EE0008561. This report was prepared as an account of work sponsored by an agency of the United States Government. Neither the United States Government nor any agency thereof, nor any of its employees, makes any warranty, express or implied, or assumes any legal liability or responsibility for the accuracy, completeness, or usefulness of any information, apparatus, product, or process disclosed, or represents that its use would not infringe privately owned rights. Reference herein to any specific commercial product, process, or service by

trade name, trademark, manufacturer, or otherwise does not necessarily constitute or imply its endorsement, recommendation, or favoring by the United States Government or any agency thereof. The views and opinions of authors expressed herein do not necessarily state or reflect those of the United States Government or any agency thereof. The authors would also like to acknowledge Universal Display Corporation for partial funding of this work.

Author Contributions

X.H. and D.F. designed and conducted the experiments. Y.L. assisted the fabrication of devices. S.R.F. supervised and supported the project. All authors contributed to the preparation of the manuscript.

Declaration of Interests

One of the authors (SRF) has an equity interest in one of the sponsors of this work (UDC). This apparent conflict of interest is under management by U-M Office of Research. The authors have applied for a patent related to the content of this paper.

References

1. Forrest, S.R. (2020). Organic electronics: Foundations to applications (Oxford University Press).
2. Li, J., Xu, L., Tang, C.W., and Shestopalov, A.A. (2016). High-Resolution Organic Light-Emitting Diodes Patterned via Contact Printing. ACS Appl. Mater. Interfaces *8*, 16809–16815.
3. Kim, C., Burrows, P.E., and Forrest, S.R. (2000). Micropatterning of organic electronic devices by cold-welding. Science (80-.). *288*, 831–833.
4. Kim, C., and Forrest, S.R. (2003). Fabrication of organic light-emitting devices by low-pressure cold welding. Adv. Mater. *15*, 541–545.
5. Ling, M.M., and Bao, Z. (2004). Thin film deposition, patterning, and printing in organic thin film transistors. Chem. Mater. *16*, 4824–4840.
6. Höppner, M., Kneppe, D., Kleemann, H., and Leo, K. (2020). Precise patterning of organic semiconductors by reactive ion etching. Org. Electron. *76*, 105357.
7. Che, X., Li, Y., Qu, Y., and Forrest, S.R. (2018). High fabrication yield organic tandem photovoltaics combining vacuum- and solution-processed subcells with 15% efficiency. Nat. Energy *3*, 422–427.
8. Meng, L., Zhang, Y., Wan, X., Li, C., Zhang, X., Wang, Y., Ke, X., Xiao, Z., Ding, L., Xia, R., et al. (2018). Organic and solution-processed tandem solar cells with 17.3% efficiency. Science *361*, 1094–1098.
9. Cui, Y., Yao, H., Zhang, J., Xian, K., Zhang, T., Hong, L., Wang, Y., Xu, Y., Ma, K., An, C., et al. (2020). Single-Junction Organic Photovoltaic Cells with

Approaching 18% Efficiency. Adv. Mater. *32*.

10. Cui, Y., Xu, Y., Yao, H., Bi, P., Hong, L., Zhang, J., Zu, Y., Zhang, T., Qin, J., Ren, J., et al. (2021). Single-Junction Organic Photovoltaic Cell with 19% Efficiency. Adv. Mater. *33*, 2102420.

11. Burlingame, Q., Huang, X., Liu, X., Jeong, C., Coburn, C., and Forrest, S.R. (2019). Intrinsically stable organic solar cells under high-intensity illumination. Nature *573*, 394–397.

12. Li, Y., Huang, X., Ding, K., Sheriff, H.K.M., Ye, L., Liu, H., Li, C.-Z., Ade, H., and Forrest, S.R. (2021). Non-fullerene acceptor organic photovoltaics with intrinsic operational lifetimes over 30 years. Nat. Commun. 2021 121 *12*, 1–9.

13. Lunt, R.R., and Bulovic, V. (2011). Transparent, near-infrared organic photovoltaic solar cells for window and energy-scavenging applications. Appl. Phys. Lett. *98*, 113305.

14. Meiss, J., Holzmueller, F., Gresser, R., Leo, K., and Riede, M. (2011). Near-infrared absorbing semitransparent organic solar cells. Appl. Phys. Lett. *99*, 10–13.

15. Li, Y., Lin, J.D., Che, X., Qu, Y., Liu, F., Liao, L.S., and Forrest, S.R. (2017). High Efficiency Near-Infrared and Semitransparent Non-Fullerene Acceptor Organic Photovoltaic Cells. J. Am. Chem. Soc. *139*, 17114–17119.

16. Li, Y., Ji, C., Qu, Y., Huang, X., Hou, S., Li, C.Z., Liao, L.S., Guo, L.J., and Forrest, S.R. (2019). Enhanced Light Utilization in Semitransparent Organic Photovoltaics Using an Optical Outcoupling Architecture. Adv. Mater. *31*,

1903173.

17. Li, Y., Guo, X., Peng, Z., Qu, B., Yan, H., Ade, H., Zhang, M., and Forrest, S.R. (2020). Color-neutral, semitransparent organic photovoltaics for power window applications. Proc. Natl. Acad. Sci. U. S. A. *117*, 21147–21154.

18. Liu, Q., Gerling, L.G., Bernal-Texca, F., Toudert, J., Li, T., Zhan, X., and Martorell, J. (2020). Light Harvesting at Oblique Incidence Decoupled from Transmission in Organic Solar Cells Exhibiting 9.8% Efficiency and 50% Visible Light Transparency. Adv. Energy Mater.

19. Bai, Y., Zhao, C., Chen, X., Zhang, S., Zhang, S., Hayat, T., Alsaedi, A., Tan, Z., Hou, J., and Li, Y. (2019). Interfacial engineering and optical coupling for multicolored semitransparent inverted organic photovoltaics with a record efficiency of over 12%. J. Mater. Chem. A *7*, 15887–15894.

20. Wang, D., Qin, R., Zhou, G., Li, X., Xia, R., Li, Y., Zhan, L., Zhu, H., Lu, X., Yip, H.L., et al. (2020). High-Performance Semitransparent Organic Solar Cells with Excellent Infrared Reflection and See-Through Functions. Adv. Mater. *32*, 2001621.

21. HKM Sheriff, Y.L.B.Q.S.F. (2021). Aperiodic optical coatings for neutral-color semi-transparent organic photovoltaics. Appl. Phys. Lett. *118*, 033302.

22. Jeong, H.I., Biswas, S., Yoon, S.C., Ko, S.-J., Kim, H., and Choi, H. (2021). Rational Design of Highly Efficient Semi-Transparent Organic Photovoltaics with Silver Nanowire Top Electrode via 3D Optical Simulation Study. Adv. Energy Mater., 2102397.

23. Huang, X., Zhang, L., Cheng, Y., Oh, J., Li, C., Huang, B., Zhao, L., Deng, J., Zhang, Y., Liu, Z., et al. (2021). Novel Narrow Bandgap Terpolymer Donors Enables Record Performance for Semitransparent Organic Solar Cells Based on All-Narrow Bandgap Semiconductors. Adv. Funct. Mater., 2108634.

24. Huang, X., Fan, D., and Forrest, S.R. (2021). Scalable semitransparent prototype organic photovoltaic module with minimal resistance loss. Org. Electron. *97*, 106276.

25. Lim, D.C., Jeong, J.H., Hong, K., Nho, S., Lee, J.-Y., Hoang, Q.V., Lee, S.K., Pyo, K., Lee, D., and Cho, S. (2018). Semi-transparent plastic solar cell based on oxide-metal-oxide multilayer electrodes. Prog. Photovoltaics Res. Appl. *26*, 188–195.

26. Dong, S., Jia, T., Zhang, K., Jing, J., and Huang, F. (2020). Single-Component Non-halogen Solvent-Processed High-Performance Organic Solar Cell Module with Efficiency over 14%. Joule *4*, 2004–2016.

27. Heo, Y.-J., Jung, Y.-S., Hwang, K., Kim, J.-E., Yeo, J.-S., Lee, S., Jeon, Y.-J., Lee, D., and Kim, D.-Y. (2017). Small-Molecule Organic Photovoltaic Modules Fabricated via Halogen-Free Solvent System with Roll-to-Roll Compatible Scalable Printing Method. ACS Appl. Mater. Interfaces *9*, 39519–39525.

28. Kutsarov, D.I., New, E., Bausi, F., Zoladek-Lemanczyk, A., Castro, F.A., and Silva, S.R.P. (2017). Fabrication of air-stable, large-area, PCDTBT:PC70BM polymer solar cell modules using a custom built slot-die coater. Sol. Energy

Mater. Sol. Cells *161*, 388–396.

29. Bernardo, G., Lopes, T., Lidzey, D.G., and Mendes, A. (2021). Progress in Upscaling Organic Photovoltaic Devices. Adv. Energy Mater. *11*.

30. Wang, G., Adil, M.A., Zhang, J., and Wei, Z. (2019). Large-Area Organic Solar Cells: Material Requirements, Modular Designs, and Printing Methods. Adv. Mater. *31*, 1–34.

31. Chen, H., Zhang, R., Chen, X., Zeng, G., Kobera, L., Abbrent, S., Zhang, B., Chen, W., Xu, G., Oh, J., et al. (2021). A guest-assisted molecular-organization approach for >17% efficiency organic solar cells using environmentally friendly solvents. Nat. Energy 2021 611 *6*, 1045–1053.

32. Lucera, L., Machui, F., Schmidt, H.D., Ahmad, T., Kubis, P., Strohm, S., Hepp, J., Vetter, A., Egelhaaf, H.J., and Brabec, C.J. (2017). Printed semi-transparent large area organic photovoltaic modules with power conversion efficiencies of close to 5 %. Org. Electron. *45*, 209–214.

33. Kubis, P., Li, N., Stubhan, T., Machui, F., Matt, G.J., Voigt, M.M., and Brabec, C.J. (2015). Patterning of organic photovoltaic modules by ultrafast laser. Prog. Photovoltaics Res. Appl. *23*, 238–246.

34. Strohm, S., Machui, F., Langner, S., Kubis, P., Gasparini, N., Salvador, M., McCulloch, I., Egelhaaf, H.J., and Brabec, C.J. (2018). P3HT: Non-fullerene acceptor based large area, semi-transparent PV modules with power conversion efficiencies of 5%, processed by industrially scalable methods. Energy Environ. Sci. *11*, 2225–2234.

35. Distler, A., Brabec, C.J., and Egelhaaf, H.J. (2021). Organic photovoltaic modules with new world record efficiencies. Prog. Photovoltaics Res. Appl. *29*, 24–31.

36. Pascual-San-José, E., Sadoughi, G., Lucera, L., Stella, M., Martínez-Ferrero, E., Morse, G.E., Campoy-Quiles, M., and Burgués-Ceballos, I. (2020). Towards photovoltaic windows: Scalable fabrication of semitransparent modules based on non-fullerene acceptorsvialaser-patterning. J. Mater. Chem. A *8*, 9882–9895.

37. Lucera, L., Machui, F., Kubis, P., Schmidt, H.D., Adams, J., Strohm, S., Ahmad, T., Forberich, K., Egelhaaf, H.J., and Brabec, C.J. (2016). Highly efficient, large area, roll coated flexible and rigid OPV modules with geometric fill factors up to 98.5% processed with commercially available materials. Energy Environ. Sci. *9*, 89–94.

38. Wang, D., Li, Y., Zhou, G., Gu, E., Xia, R., Yan, B., Yao, J., Zhu, H., Lu, X., Yip, H.-L., et al. (2022). High-performance see-through power windows. Energy Environ. Sci.

39. Röttinger, S., Schwarz, B., Schäfer, S., Gauch, R., Zimmermann, B., and Würfel, U. (2016). Laser patterning of vacuum processed small molecular weight organic photovoltaics. Sol. Energy Mater. Sol. Cells *154*, 35–41.

40. Dong, X., Jiang, Y., Sun, L., Qin, F., Zhou, X., Lu, X., Wang, W., Zhou, Y., Dong, X.Y., Jiang, Y.Y., et al. (2021). Large-Area Organic Solar Modules with Efficiency Over 14%. Adv. Funct. Mater., 2110209.

41. Ilic, B., and Craighead, H.G. (2000). Topographical patterning of chemically sensitive biological materials using a polymer-based dry lift off. Biomed. Microdevices *2*, 317–322.

42. Tan, C.P., Ri Seo, B., Brooks, D.J., Chandler, E.M., Craighead, H.G., and Fischbach, C. (2009). Parylene peel-off arrays to probe the role of cell–cell interactions in tumour angiogenesis. Integr. Biol. *1*, 587–594.

43. Tan, C.P., Cipriany, B.R., Lin, D.M., and Craighead, H.G. (2010). Nanoscale Resolution, Multicomponent Biomolecular Arrays Generated By Aligned Printing With Parylene Peel-Off. Nano Lett. *10*, 719–725.

44. Martinez, D., Py, C., Denhoff, M., Monette, R., Comas, T., Krantis, A., and Mealing, G. (2013). Polymer peel-off mask for high-resolution surface derivatization, neuron placement and guidance. Biotechnol. Bioeng. *110*, 2236–2241.

45. Defranco, J.A., Schmidt, B.S., Lipson, M., and Malliaras, G.G. (2006). Photolithographic patterning of organic electronic materials. Org. Electron. *7*, 22–28.

46. Abbas, A.S., Alqarni, S., Shokouhi, B.B., Abbas, A.S., Yavuz, M., and Cui, B. (2014). Metal and organic nanostructure fabrication by electron beam lithography and dry liftoff. Proc. IEEE Conf. Nanotechnol., 392–395.

47. Zou, C., Chang, C., Sun, D., Böhringer, K.F., and Lin, L.Y. (2020). Photolithographic patterning of perovskite thin films for multicolor display applications. Nano Lett. *20*, 3710–3717.

48. Rowell, M.W., and McGehee, M.D. (2011). Transparent electrode requirements for thin film solar cell modules. Energy Environ. Sci. *4*, 131–134.

49. Lucera, L., Kubis, P., Fecher, F.W., Bronnbauer, C., Turbiez, M., Forberich, K., Ameri, T., Egelhaaf, H.J., and Brabec, C.J. (2015). Guidelines for Closing the Efficiency Gap between Hero Solar Cells and Roll-To-Roll Printed Modules. Energy Technol. *3*, 373–384.

50. Lee, B., Lahann, L., Li, Y., and Forrest, S.R. (2020). Cost estimates of production scale semitransparent organic photovoltaic modules for building integrated photovoltaics. Sustain. Energy Fuels *4*, 5765–5772.

Table 1. Performance of 4 mm^2 PCE-10:BT-CIC:TT-FIC OPV device, and 12.8 cm^2 active area (13.34 cm^2 total area) module under simulated AM 1.5G illumination at 1 sun intensity

4 mm^2 device	J_{SC} (mA/cm^2)	V_{OC} (V)	*FF* (%)	*PCE* (%)	*APT* (%)	*LUE* (%)
opaque	23.2 ± 0.4	0.68 ± 0.01	0.69 ± 0.01	10.9 ± 0.3	-	-
ST w/o OC	17.8 ± 0.3	0.67 ± 0.01	0.70 ± 0.01	8.3 ± 0.2	22.3 ± 1.1	1.9 ± 0.1
ST w/ OC	17.1 ± 0.2	0.67 ± 0.01	0.70 ± 0.01	8.0 ± 0.2	41.8 ± 1.4	3.3 ± 0.1
neutral ST	17.4 ± 0.3	0.67 ± 0.01	0.70 ± 0.01	8.2 ± 0.1	22.8 ± 1.3	1.9 ± 0.1
module	I_{SC} (mA)			PCE_{active}[a] (%)		
opaque	36.7 ± 0.6	5.42 ± 0.02	0.66 ± 0.01	10.3 ± 0.3	-	-
ST w/o OC	28.2 ± 0.7	5.34 ± 0.02	0.64 ± 0.01	7.5 ± 0.3	22.3 ± 1.1	1.7 ± 0.1
ST w/ OC	27.2 ± 0.5	5.34 ± 0.02	0.64 ± 0.01	7.3 ± 0.2	41.8 ± 1.4	3.1 ± 0.1
neutral ST	27.4 ± 0.4	5.34 ± 0.02	0.64 ± 0.01	7.4 ± 0.2	22.8 ± 1.3	1.7 ± 0.1

[a]: *PCE* calculated based on module active area.

Figure Legends

Figure 1. **Description of the peel-off patterning method and the organic photovoltaic (OPV) module layout. (a)** Schematic illustration of the peel-off patterning procedure. **(b)** Microscopic image of PCE-10:BT-CIC blend film on a glass substrate patterned by peeling off a 10 μm wide polyimide (PI) strip. **(c)** Schematic of the series connected prototype OPV module layout comprising eight individual cells.

Figure 2. Schematic illustration of multilevel peel-off patterning scheme. (a) to **(e)** Step-by-step schematic of the fabrication process used to create series cell connection via peel-off patterning. The microscopic image in **(e)** shows the interconnection region between two individual semitransparent organic photovoltaic (ST-OPV) cells in a module, with reference to the schematic.

Figure 3. Optoelectronic properties of the ST-OPV modules with out-coupling (OC) structure. (a) Schematic of the ST-OPV device with an optical OC structure. **(b)** Current density-voltage (*J-V*) and current-voltage (*I-V*) characteristics of 4 mm^2 ST-OPV devices and modules with and without the OC structure. **(c)** External quantum efficiency (*EQE*) and **(d)** transmission and reflection spectra of the ST-OPV with and without OC structure. **(e)** Photographic image of the prototype ST-OPV module with the OC structure.

Figure 4. Optoelectronic properties of the neutral color ST-OPV modules. (a) Schematic of the neutral color ST-OPV device. **(b)** *J-V* and *I-V* characteristics of 4 mm^2 neutral color ST-OPV device and module. **(c)** *EQE*, transmission and reflection spectra of the neutral color ST-OPV. **(d)** Photographic image of the prototype, neutral color ST-OPV module.

Figure 1.

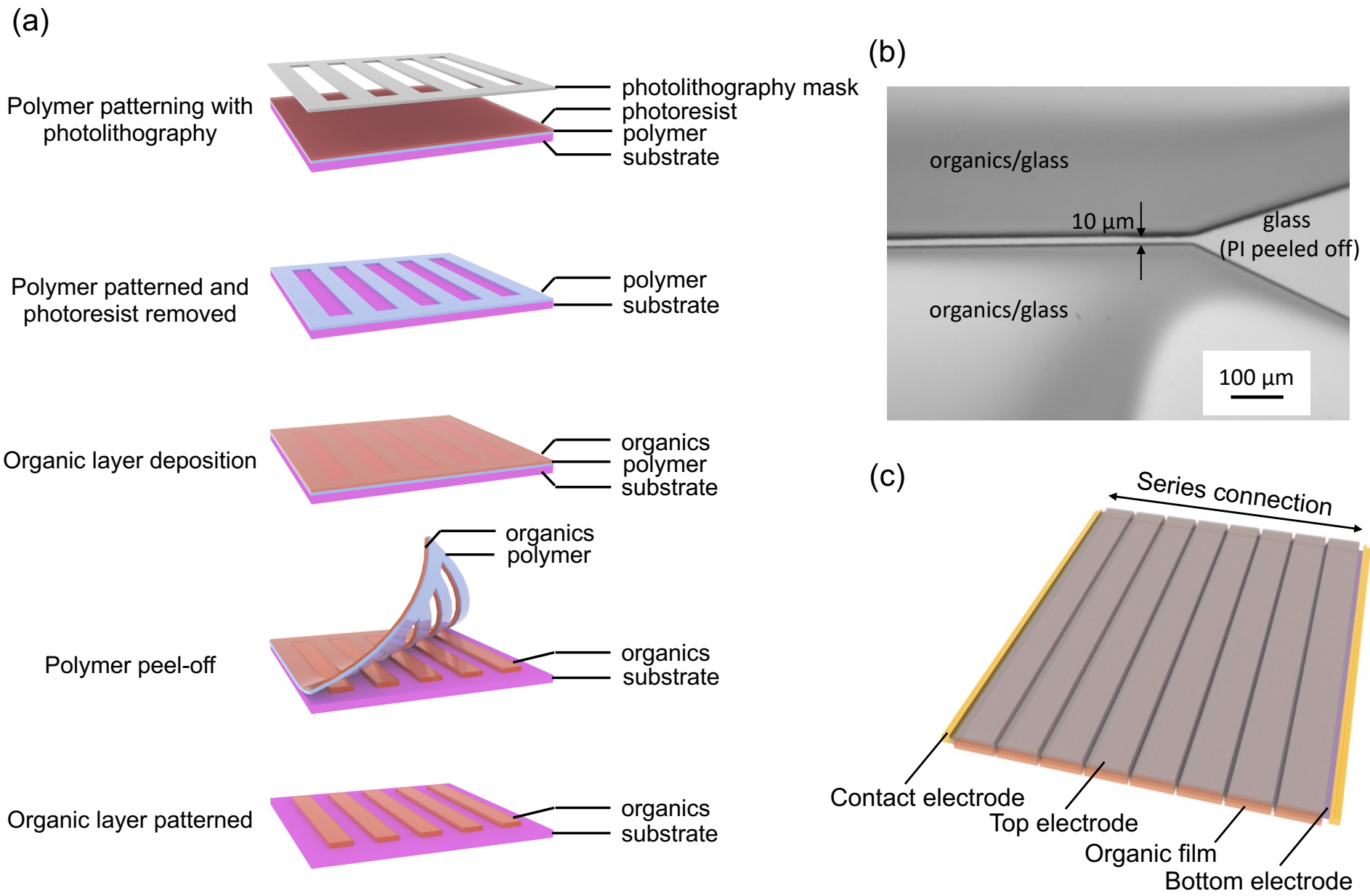
(a)
Polymer patterning with photolithography
photolithography mask
photoresist
polymer
substrate
Polymer patterned and photoresist removed
polymer
substrate
Organic layer deposition
organics
polymer
substrate
organics
polymer
Polymer peel-off
organics
substrate
Organic layer patterned
organics
substrate
(b)
organics/glass
10 µm
glass
(PI peeled off)
organics/glass
100 µm
(c)
Series connection
Contact electrode
Top electrode
Organic film
Bottom electrode

Figure 2.

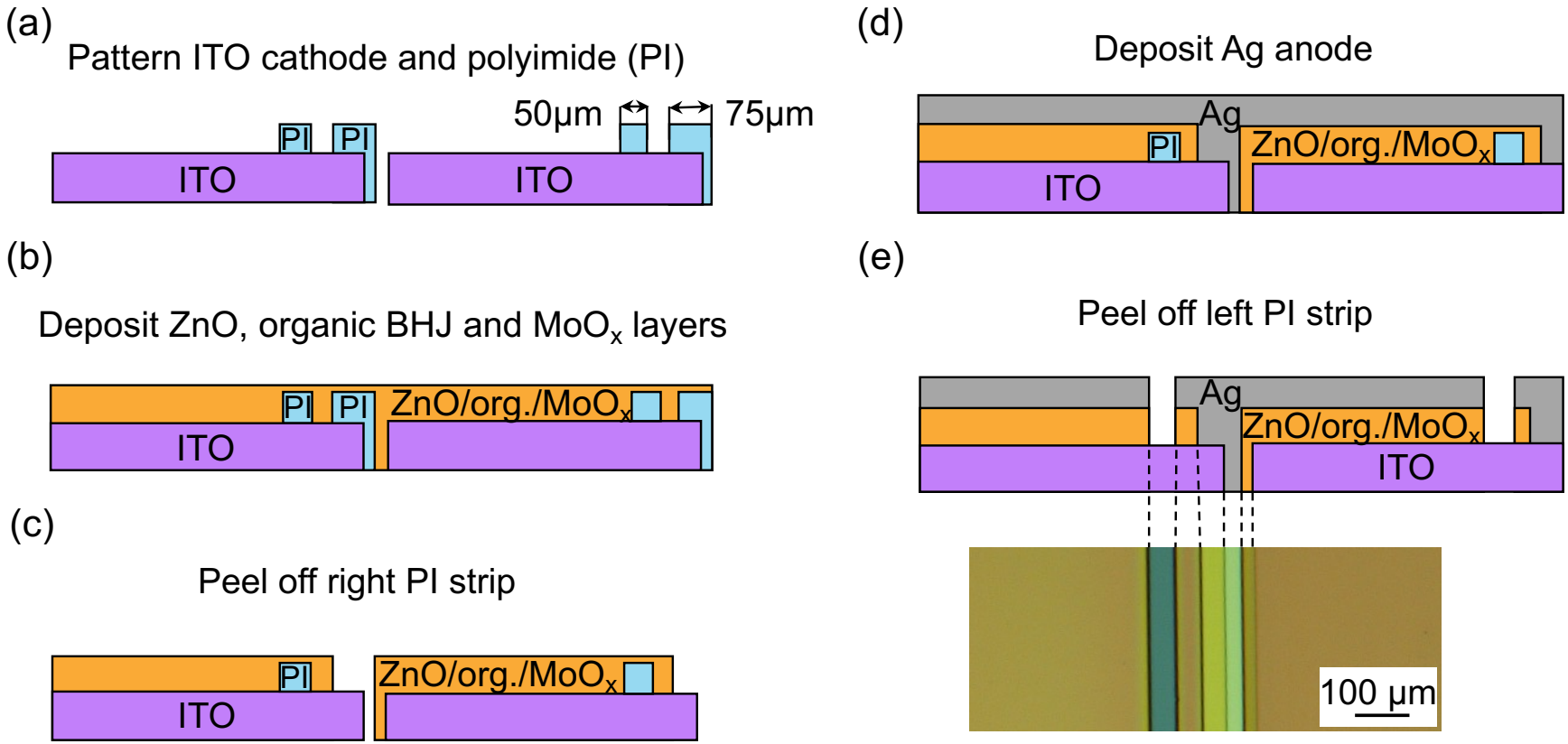
(a)
Pattern ITO cathode and polyimide (PI)
50μm
75μm
PI
PI
ITO
ITO
(b)
Deposit ZnO, organic BHJ and MoO_x layers
PI
PI
ZnO/org./MoO_x
ITO
(c)
Peel off right PI strip
PI
ZnO/org./MoO_x
ITO
(d)
Deposit Ag anode
Ag
PI
ZnO/org./MoO_x
ITO
(e)
Peel off left PI strip
Ag
ZnO/org./MoO_x
ITO
100 μm

Figure 3.

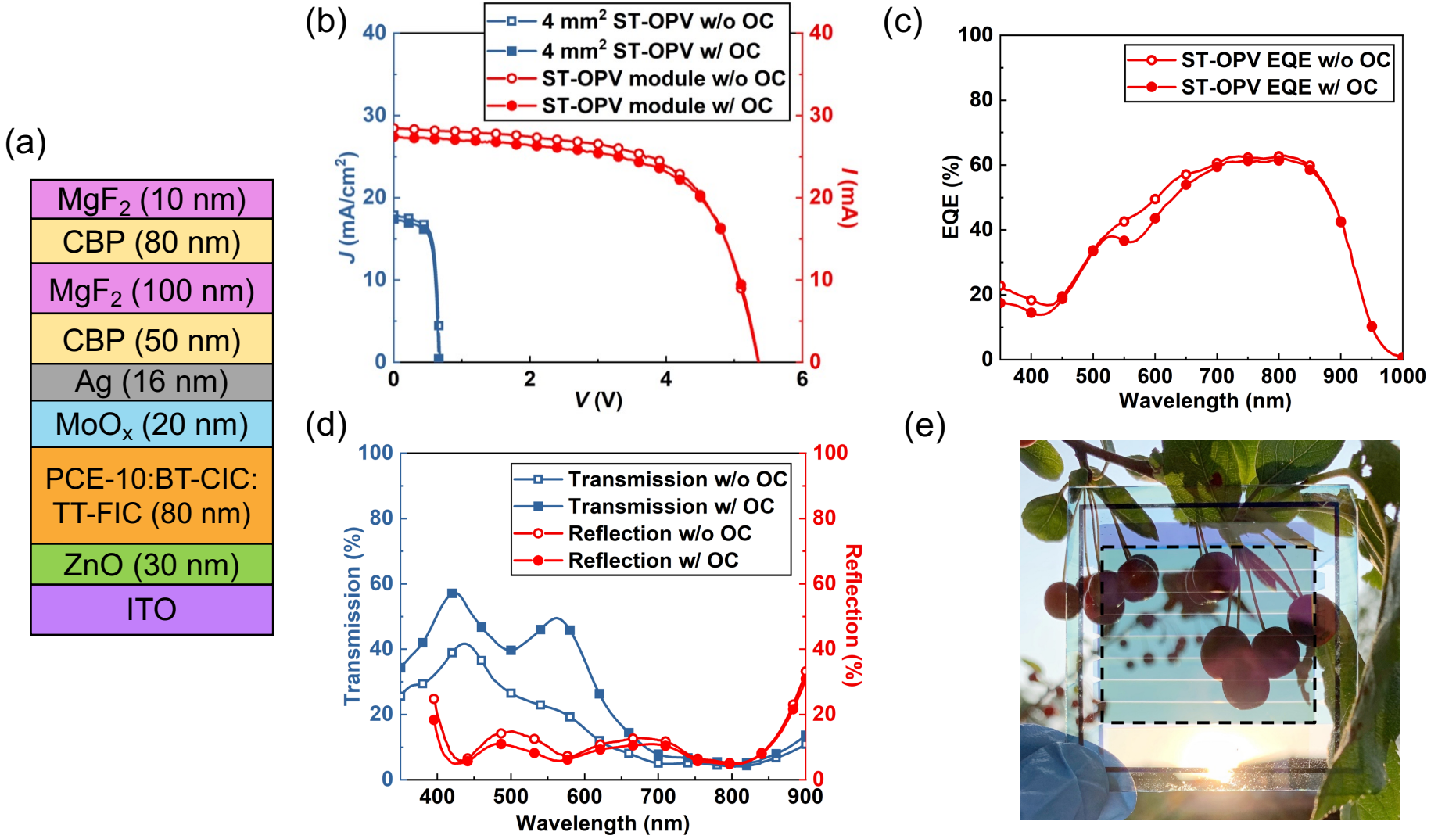
(a)
MgF2 (10 nm)
CBP (80 nm)
MgF2 (100 nm)
CBP (50 nm)
Ag (16 nm)
MoOx (20 nm)
PCE-10:BT-CIC: TT-FIC (80 nm)
ZnO (30 nm)
ITO
(b)
4 mm2 ST-OPV w/o OC
4 mm2 ST-OPV w/ OC
ST-OPV module w/o OC
ST-OPV module w/ OC
J (mA/cm2)
I (mA)
V (V)
(c)
ST-OPV EQE w/o OC
ST-OPV EQE w/ OC
EQE (%)
Wavelength (nm)
(d)
Transmission w/o OC
Transmission w/ OC
Reflection w/o OC
Reflection w/ OC
Transmission (%)
Reflection (%)
Wavelength (nm)
(e)

Figure 4.

(a)

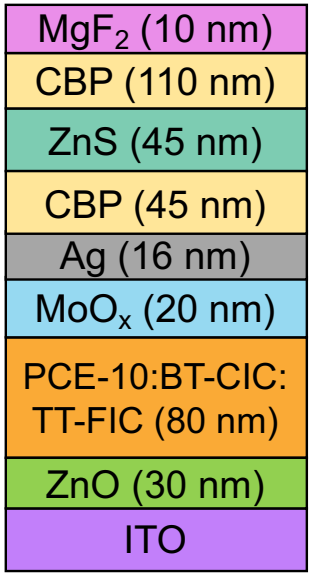

(b)

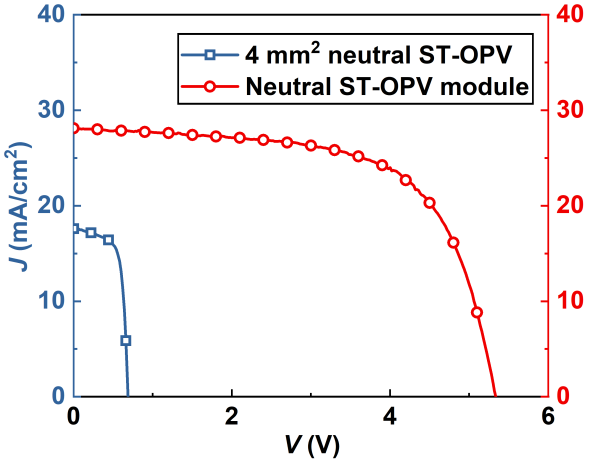

(c)

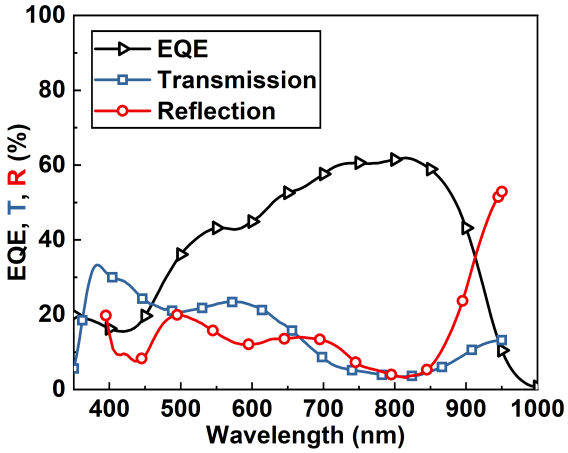

(d)